lubricants

MDPI

Article

Effect of Loads on Tribological Performance of Rubber Seals at Floating Wind Power in Deep Sea

Guibin Tan [1,2,*], Cheng Zhou [1,2], Jiantao Liang [1,2], Guangjing Huang [3], Zhixing Wang [1,2] and Xing Huang [1,2,4]

[1] School of Electromechanical Engineering, Guangdong University of Technology, Guangzhou 510006, China
[2] Guangdong Provincial Key Laboratory of Advanced Manufacturing Technology for Marine Energy Facilities, Guangzhou 510006, China
[3] CATO Co., Ltd., Dongguan 523000, China
[4] Guangzhou Mechanical Engineering Research Institute Co., Ltd., National Engineering Research Center of Rubber & Plastic Sealing, Guangzhou 510535, China
* Correspondence: tanguibin@gdut.edu.cn

Abstract: The main shaft seal of offshore wind power equipment is one of the key components of wind power systems. However, wear issues between the seals and the main shaft caused by the intrusion of particulate matter in the environment have become a key factor affecting the service life of the equipment. To improve the surface performance of the main shaft, this study used laser cladding technology to prepare an Fe55 coating on the surface of QT-500 components. Through the wear experiments on HNBR seal pairs with the main shaft under different load conditions, this study thoroughly investigated the impact of the coating on frictional coefficients, wear mechanisms, and the wear morphology of metal surfaces. The experimental results show that the average hardness of the Fe55 coating is 533 HV, which is about 2.3 times the hardness of the substrate, and as the loading force increases, the wear form of the QT-500 metal changes from being dominated by pits to being dominated by furrows. In contrast, the wear form of the Fe55 coating is more inclined to furrows, and no pit formation is observed, indicating that the coating has improved the wear resistance of the surface. The frictional coefficient of the HNBR pair with the metal decreases with increasing load, and the frictional coefficient of the coating is lower than that of the substrate. As the loading increases, the wear morphology of the rubber surface transitions from furrows to pits, and the wear mechanism becomes abrasive wear.

Keywords: rubber tribology; seals; offshore wind power; abrasive wear; laser cladding

check for updates

Received: 3 January 2025
Revised: 23 February 2025
Accepted: 26 February 2025
Published: 3 March 2025

Citation: Tan, G.; Zhou, C.; Liang, J.; Huang, G.; Wang, Z.; Huang, X. Effect of Loads on Tribological Performance of Rubber Seals at Floating Wind Power in Deep Sea. *Lubricants* **2025**, *13*, 111. https://doi.org/10.3390/lubricants13030111

Copyright: © 2025 by the authors. Licensee MDPI, Basel, Switzerland. This article is an open access article distributed under the terms and conditions of the Creative Commons Attribution (CC BY) license (https://creativecommons.org/licenses/by/4.0/).

1. Introduction

The global energy landscape is undergoing significant transformation, driven by the rising demand for renewable energy [1]. Offshore wind power, illustrated in Figure 1, is a clean and efficient energy source that is rapidly developing and has become a crucial component of the energy sector. Mechanical drive chain failures account for up to 30% of major wind turbine incidents, and the reliability of the drive chain directly affects the overall quality of wind turbine products [2,3]. As shown in Figure 2, the sealing interface plays a critical role; failures in the main shaft seal can severely impact the reliability and stability of the entire wind turbine system [4].

In the challenging marine environment, even with rubber seals in place, particles and debris can infiltrate the sealing interface, resulting in significant abrasive wear [5]. Additionally, eccentricity reduces the axial gap between the dynamic and static rings of the main seal, which increases the compression of the seal lip against the main shaft. As a

result, this heightened compression elevates friction, leading to accelerated wear of the seal lip and ultimately decreasing the seal's service life [6]. At the same time, different depths of wear grooves are left on the main shaft surface of the seal track [7]. When the wear grooves reach a certain extent, the sealing compression of the seal lip can no longer compensate for the wear, which seriously threatens the normal operation of the main drive system. Qin et al. [8] studied the auxiliary wear of different sizes (nano to micron) particles in the gear oil and found that nano SiO_2 particles would reduce the oil film strength or extreme pressure performance of the gear oil, thus aggravating the wear of industrial gearboxes. Zuo et al. [9] combined the effect of hysteresis to analyze the tribological mechanism of HNBR under abrasive wear conditions, dividing the total frictional coefficient into adhesion, hysteresis, and abrasive components. Qin Zhou [10] established a force model for individual particles at the interface between soft rubber and hard metal. She analyzed three typical types of particle breakage, including grinding, partial crushing, and complete crushing. Under high load, more particles are crushed, while under low load, the edges of particles are more prone to shear failure.

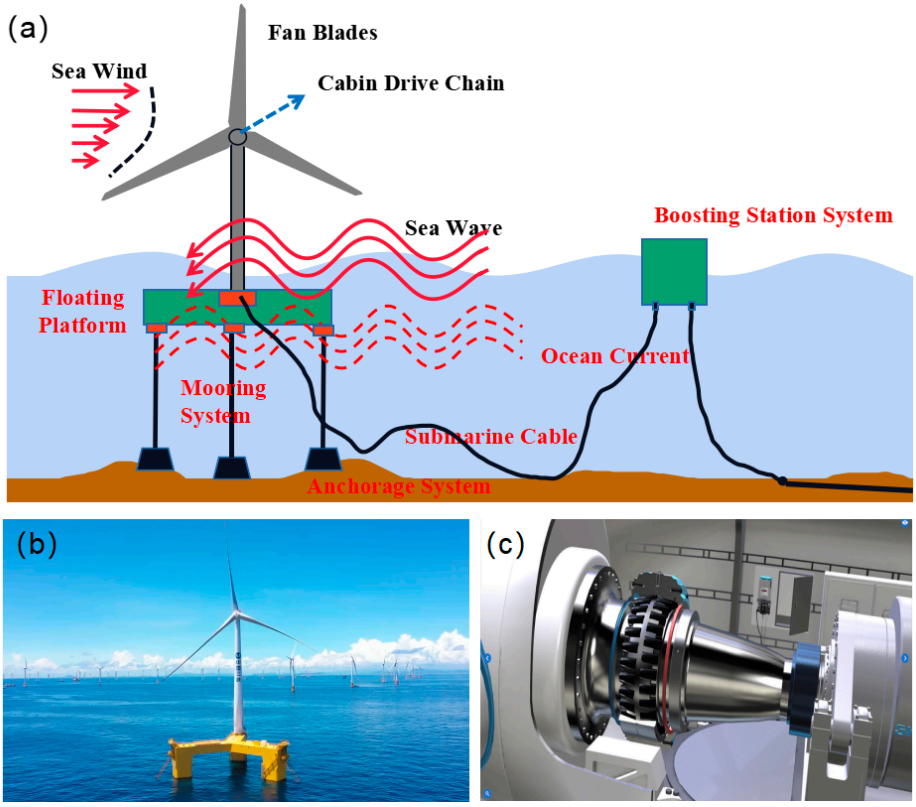


Figure 1. Common problems of rubber seals at floating wind power. (**a**) The floating system of wind power. (**b**) The main construction at deep sea. (**c**) The rubber seals and the shafting rotor.

When dealing with seal failure issues, the traditional approach of replacing seals can be both costly and complex, resulting in long downtimes and significantly impacting the economic performance of wind farms. To enhance maintenance efficiency and lower costs, laser cladding technology has been introduced for repairing the main shafts of wind turbines. This technology offers high precision, a low heat-affected zone, and excellent material compatibility, making it an increasingly important method for the repair of mechanical components [11,12].

This paper addresses the typical conditions of main shaft sealing devices used in deep-sea wind power equipment, constructing a tribological model specifically for rotating shaft lip seals. Using the CFT-I testing rig, tribological experiments were conducted to assess the

frictional, lubricating, and wear characteristics of the main shaft and HNBR (hydrogenated nitrile rubber). Furthermore, to investigate the repair and re-manufacturing effectiveness of Fe55 coating on the wear traces of sealing tracks for offshore wind turbines, the performance of HNBR/Fe55 rotating seals under abrasive conditions was experimentally evaluated. QT-500 ductile cast iron, the same material utilized for the main shaft of floating offshore wind turbines, served as the substrate for laser cladding repair, aimed at evaluating its practical application in harsh marine environments. Through these experimental studies and performance tests, changes in wear resistance and service life of the sealing pair following laser cladding repair were assessed, intending to provide a robust scientific foundation and technical support for the reliability of offshore wind power main shaft sealing systems, while fostering the continuous advancement and development of offshore wind power technology.

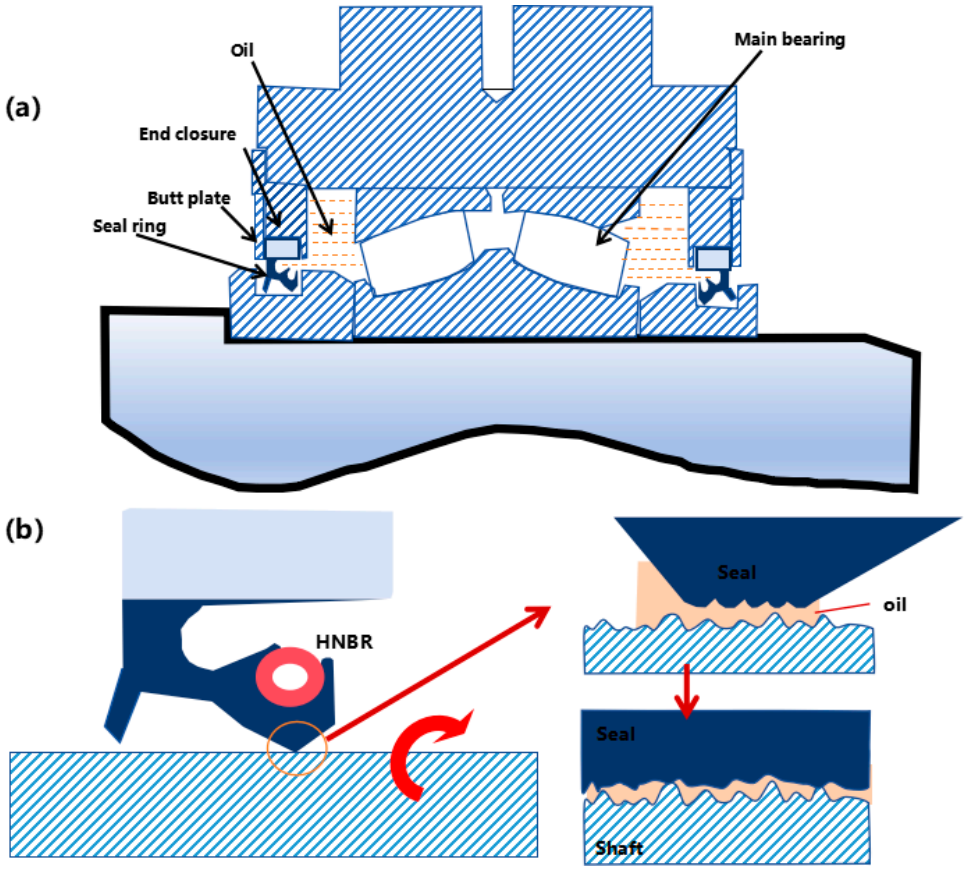


Figure 2. (**a**) Schematic diagram of the rubber seals (HNBR) at the main shaft for the wind turbine. (**b**) The rough soft-contact model of the seal pair.

2. Experimental Procedure

2.1. Soft Lubrication Testing Rig

This study selects a pin-on-disk pair of HNBR samples and QT-500 as the research object. The CFT-I pin disk multifunctional material surface performance tester is used, as shown in Figure 3. Under a certain axial load, the friction pair can slide relatively. The axial load is applied to the pin friction pair by the loading mechanism.

In order to study the wear degradation law of metal shaft and HNBR under different working conditions, the metal shaft material and rubber material were used as upper and lower specimens for reciprocating friction, and their appearance and motion patterns are shown in Figure 3a. As shown in Figure 3b,c, the upper specimen material is the metal of QT-500 and Fe55-coated pin with a bottom diameter of 12 mm. The lower specimen

is a HNBR sheet with a surface roughness *Ra* of approximately 1.35 µm. Each sample is cut into a nearly 40 mm by 40 mm square thin sheet, with a thickness of 2 mm. The HNBR samples were provided by the National Engineering Research Center of Rubber & Plastic Sealing, China Guangzhou Mechanical Engineering Research Institute Co., Ltd. (Guangzhou, China). The basic parameters of HNBR can be found in Table 1. In the offshore wind electric spindle seal environment, particles around 80 um are the most common, so the particle size of SiO_2 particles is #200 orders and the average particle size is about 74 µm [9].

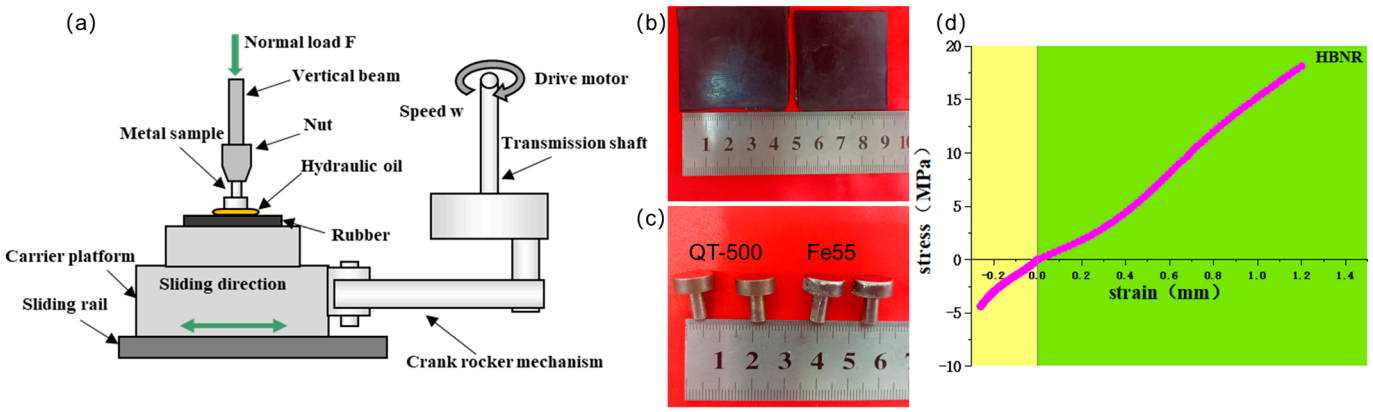


Figure 3. Schematic diagram of the tribological testing rig. (**a**) CFT-I. (**b**) The HNBR samples. (**c**) Steel samples. (**d**) The testing data of the HNBR stress–strain curve.

Table 1. Main parameters of the HNBR material.

Density	Young's Modulus (MPa)	Poisson Ratio	Tensile Strength (MPa)	Elongation At Break (%)	Hardness (Shore A)
1.24 g/cm^3	7.003	0.465	20.4 MPa	295%	72.3 Shore A

The cross-sectional morphology of the Fe55 laser cladding coating is illustrated in Figure 4a–c. As observed in these figures, there is a noticeable bright white band between the Fe55 coating and the QT-500 substrate, indicating effective metallurgical bonding. No pores, cracks, or other defects were detected in the coating, which suggests that it is of overall good quality. It can also be seen from Figure 4d that the laser cladding coating microstructure is mainly composed of equiaxed crystals and cellular crystals. Figure 4e displays the results from a Vickers micro-hardness test conducted on the Fe55 coating. The micro-hardness tester was set with a load of 200 g and a dwell time of 10 s. For each sample, 5 to 10 measurement points were taken, and the average of these results was calculated as the final hardness value. The micro-hardness of the cladding layer shows a significant improvement compared to the substrate, measuring approximately 2.3 to 2.5 times greater. Figure 4f shows the XRD pattern of the Fe55 laser cladding coating. The main phases in the coating are the body-centered cubic (BCC) structure of α-Fe, the (Fe, Ni) and Fe-Cr solid solutions, as well as Fe-Cr-Ni compounds.

The QT-500 ductile iron commonly used in wind turbine spindles was selected as the substrate for laser cladding in this experiment, and its chemical composition is shown in Table 1. The cladding powder is Fe55 stainless steel powder, and its nominal composition is shown in Table 2.

In this experiment, we utilized #200 gear oil, which exhibits a viscosity index of 121, indicating its ability to maintain stable viscosity across a range of temperatures. Specifically, the kinematic viscosity of this gear oil is measured to be 332.5 mm^2/s at 40 °C and 29.42 mm^2/s at 100 °C. The contact loads tested were 60 N, 70 N, 80 N, and 90 N. Each

experiment was conducted for 30 min at a reciprocating frequency of 300 cycles per minute. Additionally, under abrasive conditions, a lubricating fluid consisting of #220 gear oil mixed with 0.1 g/mL SiO_2 particles was prepared. Friction experiments were performed under higher load conditions of 80 N, 100 N, 120 N, and 140 N, with a reciprocating frequency of 300 cycles per minute and a stroke length of 4 mm. Each of these experiments was also set for a duration of 30 min.

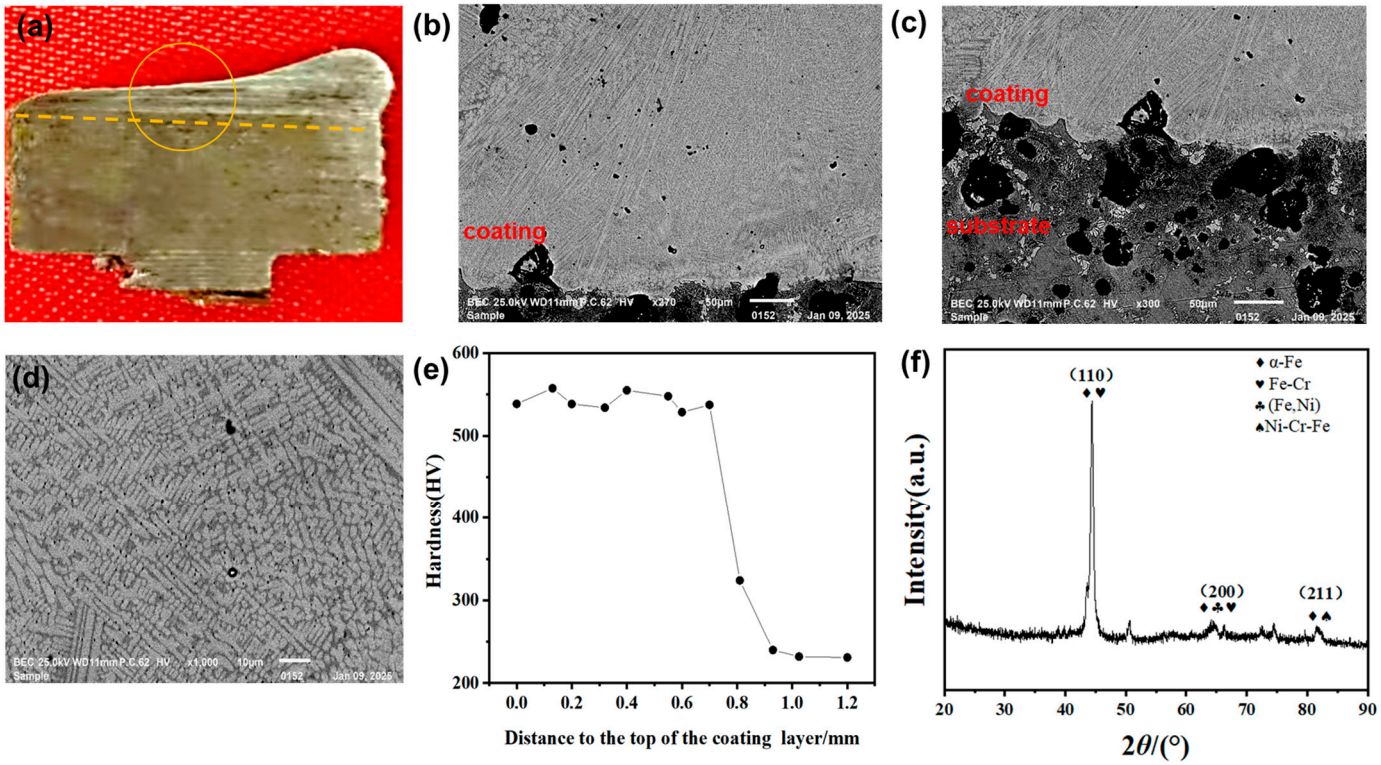


Figure 4. (**a**) The cross-section of Fe55 cladding coating. (**b**,**c**) The cross-sectional morphology of Fe55 cladding coating. (**d**) Microstructure of the Fe55 laser cladding coating. (**e**) The hardness distribution of Fe55 cladding coating. (**f**) The XRD pattern of Fe55 cladding coating.

Table 2. Chemical composition of QT-500 and Fe55 powder (wt.%).

Sample	C	Si	Mn	P	S	Nb	B	Cr	Ni	Mo	Mg	Cu
QT-500	5.57	2.08	0.505	0.027	0.010	-	-	-	-	-	0.056	0.656
Fe55	0.18	0.85	0.57	-	-	0.28	0.81	18.98	2.76	0.89	-	-

2.2. Numerical Simulation Analysis of Offshore Wind Power Lip Seals

To explore the reasons for the failure of lip seals at offshore wind power under eccentric conditions [13], this paper uses the finite element method (FEM) to establish a dynamic simulation model of the friction pair of marine wind power lip seals [13]. The simulation results are shown in Figure 5a. As shown in Figure 5b, due to the impact of eccentricity on the interference fit, as the eccentricity increases, the contact width on the side where the interference fit of the oil seal increases also increases, reducing stress concentration, which results in a decrease in peak contact pressure; on the other side where the interference fit decreases, the contact width decreases, but due to the compensation of the spring radial force, the change in peak contact pressure is not significant. As shown in Figure 5c, on the side where the interference fit increases, the radial force increases with the increase in eccentricity. As shown in Figure 5d, at the critical section from 108° to 180°, the friction

force is high. In summary, the lip seal is more prone to wear and failure under static eccentric conditions.

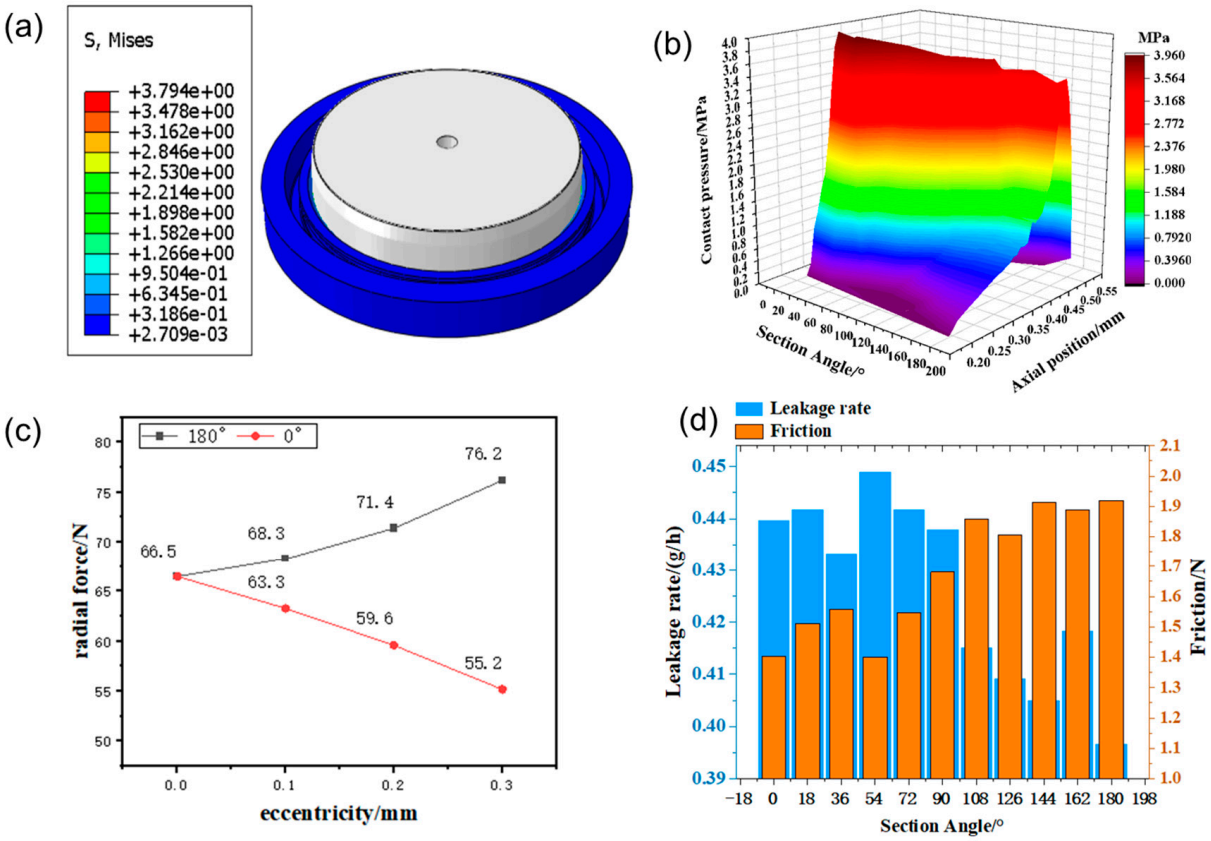


Figure 5. The numerical simulation results of rubber seals at wind power. (**a**) Mises stress cloud diagram of lip seal friction pair. (**b**) The contact stress cloud diagram of seals. (**c**) Diagram of radial force variation with eccentricity. (**d**) Leakage rate and friction force of each section.

3. Results

3.1. Tribological Properties of Oil-Lubricated Lip Seal Friction Pair Material

3.1.1. Frictional Coefficient Analysis Under Oil Lubrication

The coefficient of friction of the HNBR under oil lubrication with different loads is shown in Figure 6. The HNBR shows a relatively stable frictional coefficient under different load conditions. At the 60 N load, after the frictional coefficient passes a short rise phase (0–5 min), the frictional coefficient begins a slow decline phase (5–15 min) and then enters a stable phase (15–30 min). With the rise in the load, at 70–90 N, the frictional coefficient showed a similar trend, namely the frictional coefficient first slowly rises, and then the friction around 10 min levels off. This is because at the beginning of contact, the metal shaft and the HNBR surface meet between a small rough peak, so the frictional coefficient is increased; this rising stage belongs to the run-in stage. With the continuation of the friction process, the removed dust of the HNBR matrix is added to the friction interface as a third body. When the removal and generation of the friction dust achieves dynamic balance, the frictional coefficient begins to remain stable, and the stability stage is also known as the stable friction stage. Since the frictional coefficient at each load reached the stable stage after 15 min, the mean of the frictional coefficient of 15–30 min was taken as the average frictional coefficient of each group of experiments, and the average frictional coefficient under 60 N, 70 N, 80 N, and 90 N loads was 0.46, 0.39, 0.32, and 0.28, respectively.

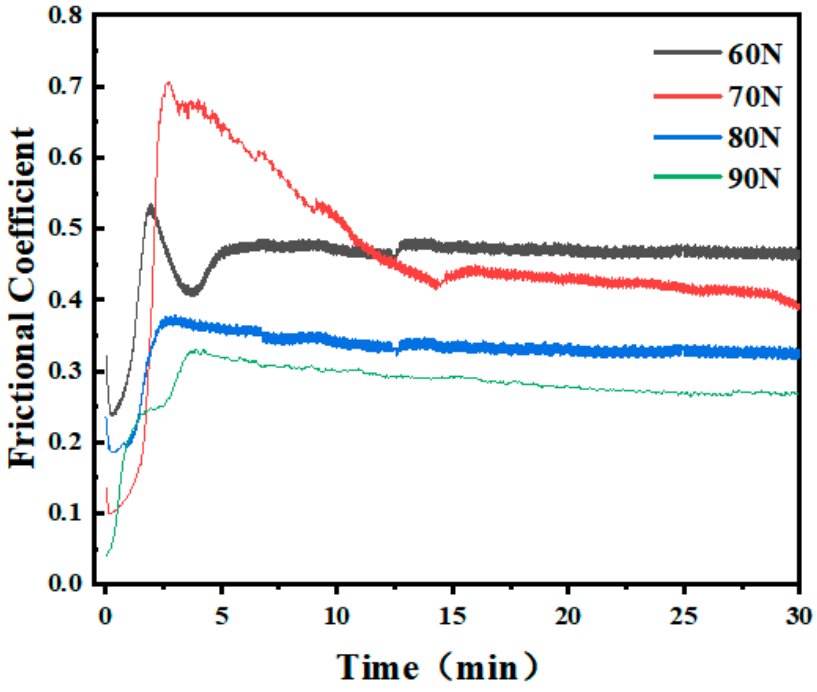


Figure 6. Average frictional coefficient under different contact loads under oil lubrication.

3.1.2. Surface Wear and Morphology Analysis

To reveal the friction and wear mechanisms of HNBR under oil lubrication at various loads, the surface micro-morphology at low and high magnifications under each load was observed using a scanning electron microscope. As shown in Figure 7, Figure 7a–d are electron microscope photos corresponding to loads of 60 N, 70 N, 80 N, and 90 N, respectively. After the friction process, there are distinct furrows on the surface of the HNBR, and the furrow phenomenon gradually diminishes with the increase in load.

As shown in Figure 7a,a1, when the load is 60 N, the worn HNBR surface showed a shallow furrow and many sticky rubber and block; this is typical wear, due to the HNBR's own mechanical properties being poor. The resistance to creep and shear ability is insufficient, and the rubber surface can be easily damaged by the surface of the metal pins' rough peak. At a load of 70 N, as shown in Figure 7b,b1, a deeper furrow appeared and only a small number of fine clumps of rubber chips were seen, which significantly decreased roughness compared to 60 N. When the load increased to 80 N, as shown in Figure 7c,c1, the rubber surface was smooth and dense with only a small amount of furrow, and many small holes appeared on the surface, probably due to fatigue peeling at higher loads. At a 90 N load, as shown in Figure 7d,d1, the friction surface is smooth and dense without obvious scratches, and the HNBR basically does not wear. This is because with the increase in the load, the contact surface of the metal pin and the rubber increase, and the rough peak bulge of the metal pin gradually filled with the rubber. It can be found that in the 60–90 N load range, on the one hand, the increase in the load reduces the frictional coefficient, and on the other hand, the wear degree of HNBR is lower and lower. With the increase in the load, the rubber surface is further squeezed, and the wedge gap is formed between the steel and the rubber. Under the wedge effect, the gear oil forms a more stable fluid dynamic pressure lubrication film, and the pressure contact in the contact area is more uniform, which effectively prevents the direct contact between the metal and rubber and plays a role in reducing the friction resistance and reducing the wear of rubber.

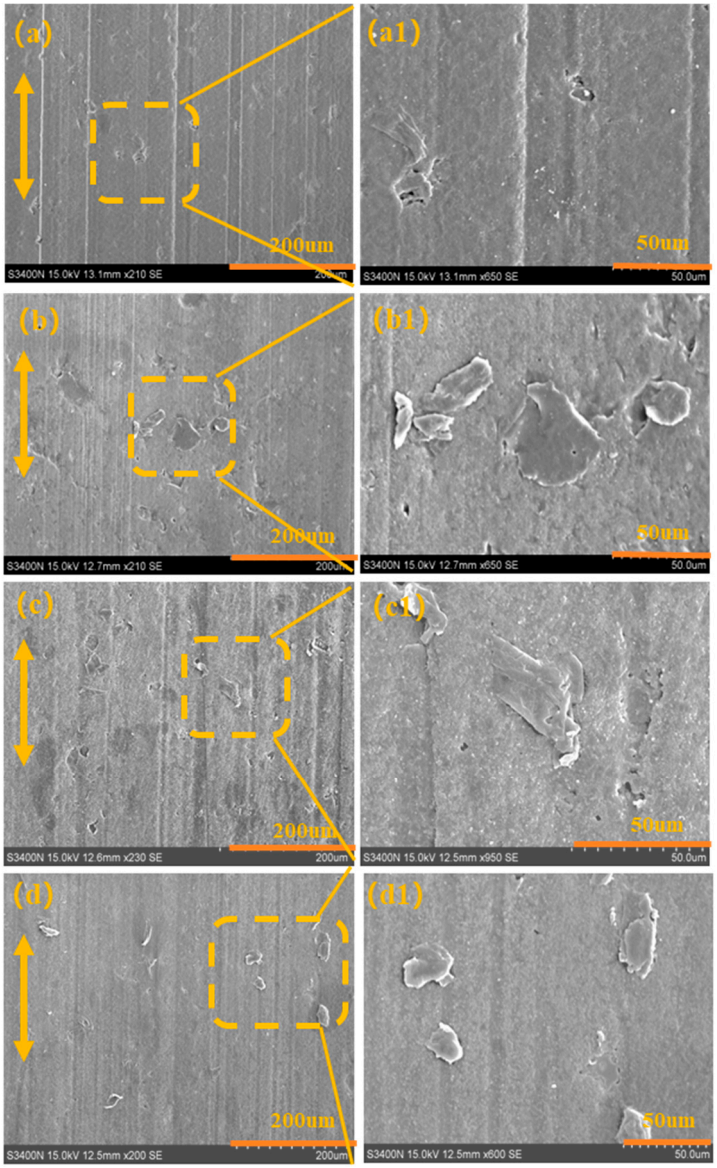


Figure 7. Surface wear phenomenon of rubber seals at oil lubrication: (**a**) 60 N, (**b**) 70 N, (**c**) 80 N, (**d**) 90 N.

3.2. The Influence of Sand Particles on the Friction Pair of Lip Seals

3.2.1. Frictional Coefficient Analysis Under Abrasive Conditions

Figure 8a–d presents the variation of friction coefficient over time for the QT-500/HNBR pair and the Fe55 coating/HNBR pair under various axial loads. Under lubricating conditions with sand particles, the variation curve of the frictional coefficient for the tribological pair can be divided into two main stages: an initial decreasing phase and a subsequent steady phase. Upon examining the frictional coefficient variation curve, it is observed that in a lubricating environment containing particles, the frictional coefficient rapidly increases initially (within the first 5 min) and then gradually decreases, eventually stabilizing with a similar pattern of temporal variation. This initial decline is closely related to the continuous formation of the lubricating oil film and the wear of surface micro-asperities and processing textures. Once the frictional coefficient enters the steady phase, a stable layer of lubricating oil film is formed on the contact surface.

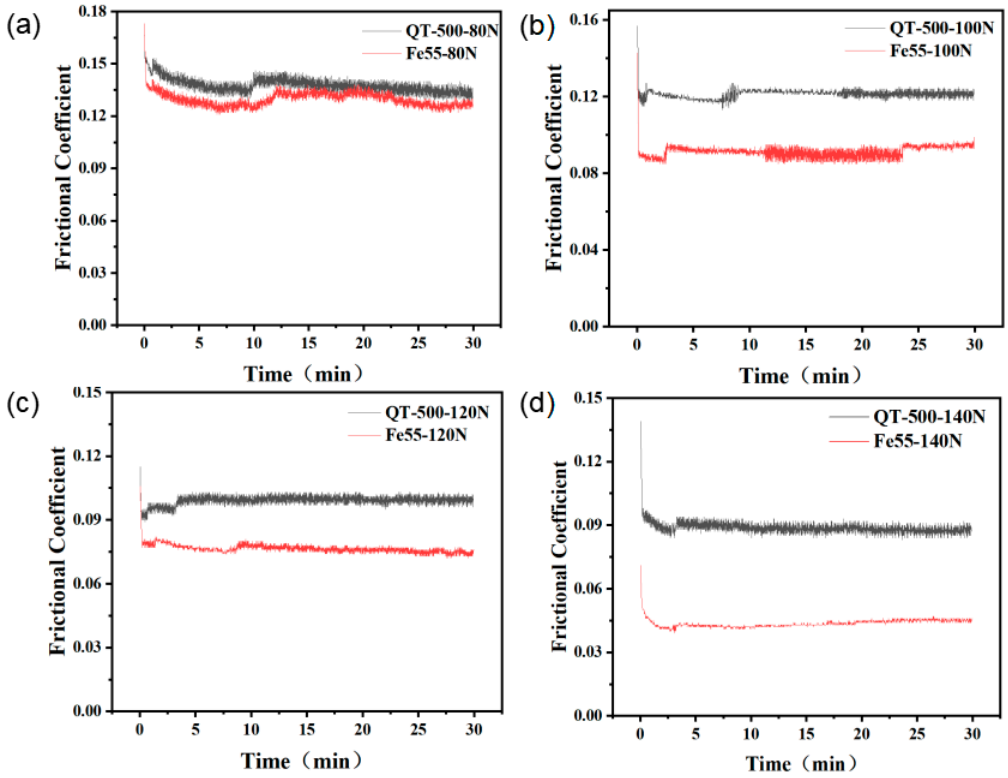


Figure 8. The variation curve of frictional coefficient over time under different axial loads.

Figure 9 presents the average frictional coefficient during the steady phase, indicating that the average frictional coefficient tends to decrease with an increase in axial load. By selecting the frictional coefficient during the steady phase as the average value, the average frictional coefficients for the QT-500/HNBR pair under loads of 80 N, 100 N, 120 N, and 140 N are found to be 0.14, 0.12, 0.10, and 0.07, respectively. For the Fe55 coating/HNBR pair, the average frictional coefficients are 0.13, 0.09, 0.08, and 0.04, respectively. The average frictional coefficient shows a downward trend with increasing load. The frictional coefficient for the Fe55 coating/HNBR pair is lower than that for the QT-500/HNBR pair, likely due to the Fe55 coating causing less deformation and energy loss during the contact process, thereby reducing the frictional coefficient.

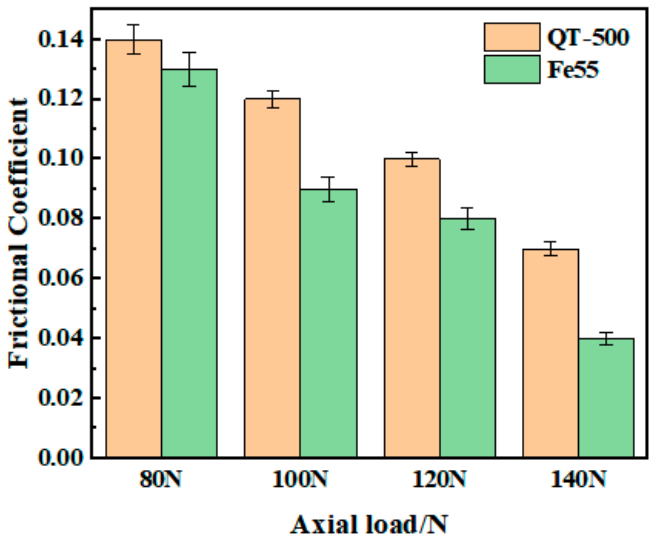


Figure 9. Average coefficient of friction between the QT-500 and Fe55 coatings under different loading conditions.

3.2.2. Surface Wear Morphology

Figure 10a,a1–d,d1 show the SEM images of the worn surface of HNBR specimens in the HNBR/QT-500 pair, and Figure 10e,e1–h,h1 show the SEM images of the worn surface of HNBR specimens in the HNBR/Fe55 pair under different loads. Observations of the worn surfaces indicate the presence of various wear mechanisms. Regarding lubrication, Figure 10 does not show the wavy features caused by dry friction of rubber materials, indicating good lubrication at the contact surface during the test. However, the hard particles present in the test were much larger than the thickness of the oil film, meaning these particles could penetrate the oil film and directly interact with the contact surface. Due to the presence of these hard particles, the main wear mechanism was abrasive wear. As hard particles rolled or slid between the contact surfaces, they caused cutting or peeling of the material. Abrasive wear usually led to noticeable scratches and pits on the surface.

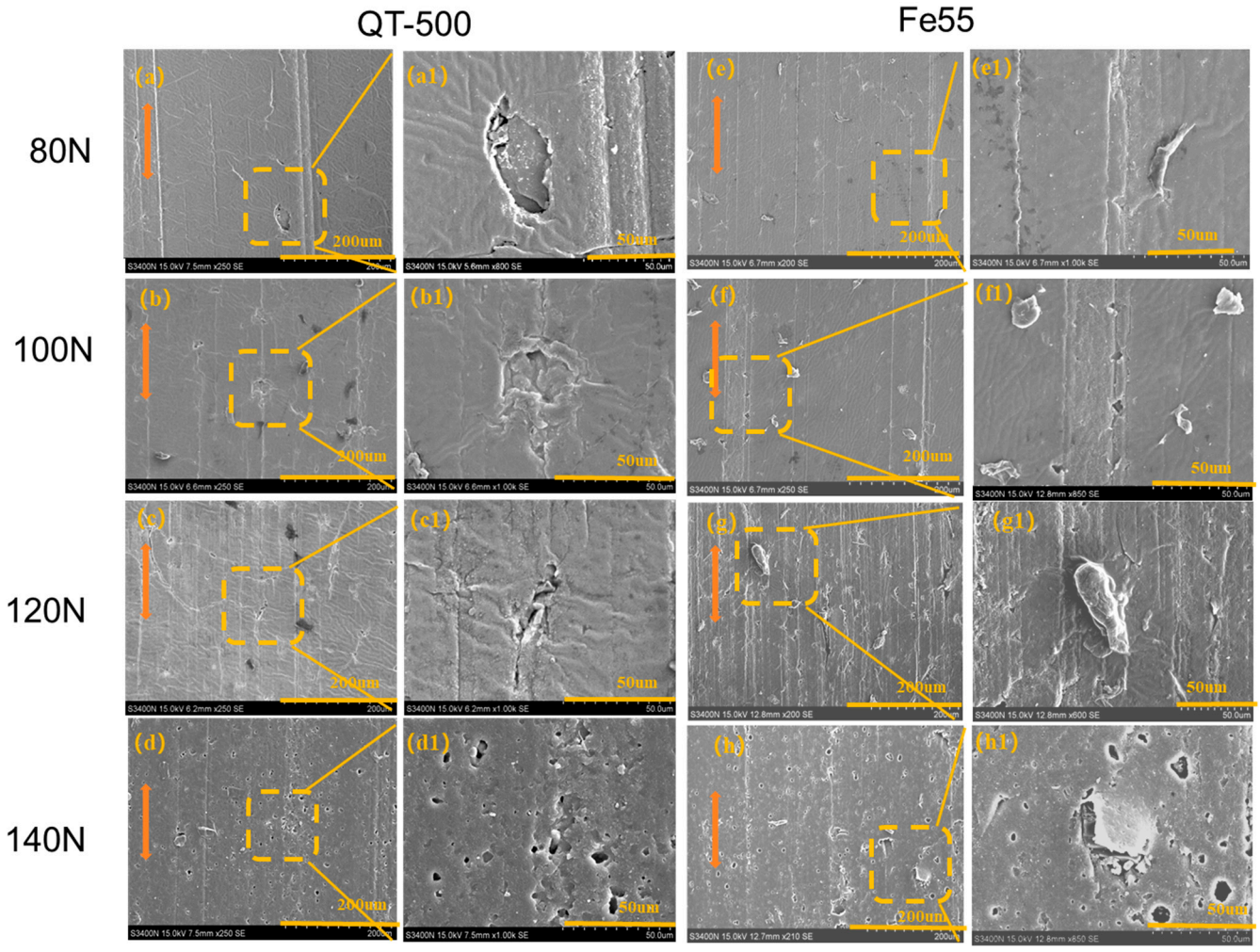


Figure 10. The worn morphology of rubber surface of HNBR/QT-500 pairs and HNBR/Fe55 pairs under the different loads.

When the axial load is 80 N, as shown in Figure 10a,a1,e,e1, the main damage to the wear surface is the plowing grooves caused by the plowing effect of hard particles [14]. Currently, the axial load is relatively small and not sufficient to cause large-scale surface peeling or other complex damage to the rubber surface. The rubber surface matrix can remain intact. As the axial load increases to 100–120 N, as shown in Figure 10b,c,f,g, with the increase in the axial load, the pressure exerted by hard particles and metal rough peaks on the rubber surface increases. The greater pressure makes the plowing effect of hard

particles on the rubber surface stronger, so the density and depth of the plowing grooves on the wear surface increase accordingly. As shown in Figure 10g1, adhesive hydrogenated nitrile rubber wear debris on the surface. This is because during the intense friction process, the hard particles and metal rough peaks exert squeezing and scraping effects on the hydrogenated nitrile rubber surface, causing part of the rubber surface layer to be extruded and peeled off. The root part is not completely cut off and is squeezed onto the rubber surface under high load to form flake-shaped wear debris. When the axial load further increases to 140 N, as shown in Figure 10d,h, the sand particles are embedded in the wear surface, continuously causing micro-cutting damage. The damage on the wear surface changes from plowing grooves to pits.

3.2.3. Metal Surface Morphology Wear

Figure 11a–d shows the wear morphology of the QT-500 metal surface under different loads, and Figure 11a1–d1 shows the 3D profiles of the QT-500 metal surface under different loads. When the test load is 80 N, as shown in Figure 11a,a1, the metal wear surface is covered with numerous pits formed by the rolling of abrasive particles [15], accompanied by slight furrows. At this stage, the wear morphology is mainly characterized by pits and minor furrows. When the test load is 100–120 N, as shown in Figure 11b,b1,c,c1, with the increase in load, the abrasive particles penetrate the rubber surface and roll within the friction interface while also sliding and plowing the metal surface. This friction state is known as the "grinding wheel effect" [16,17], leading to furrow-shaped damage on the metal surface.

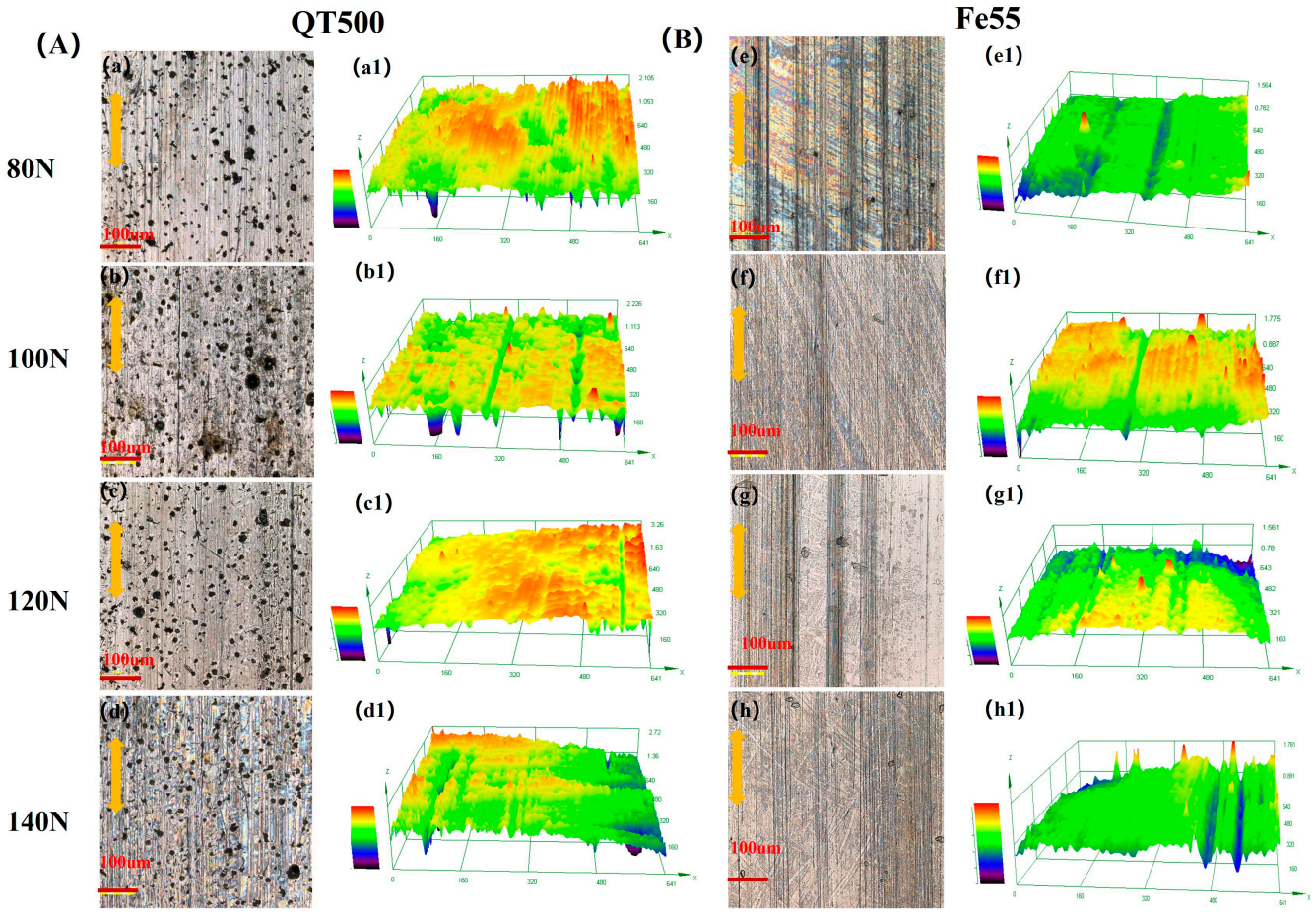


Figure 11. The microscope images and 3D profiles. (**A**) Fe55 coating surface wear morphology. (**B**) QT-500 surface wear morphology.

The number of pits on the QT-500 metal surface increases, and the furrows deepen. When the test load is 140 N, as shown in Figure 11d,d1, with the further increase in axial load, more abrasive particles embed into the rubber surface and slide against the metal surface. Under high load, the abrasive particles exert greater shear and compressive stress on the metal surface, resulting in predominantly furrow wear morphology.

Figure 11e–h shows the wear morphology of the Fe55 coating surface under different loads, and Figure 11e1–h1 shows the 3D profiles of the Fe55 coating surface under different loads. As shown, with the increase in load, the furrows on the coating surface gradually deepen, and no pits are observed. Laser cladding treatment can improve the hardness and wear resistance of the metal surface, reducing the occurrence of wear, and the wear form tends to be localized plastic deformation, forming furrow-like surfaces.

The characteristic dimensions of the QT-500 and Fe55 coating metals are shown in Figure 12. As the load increases, the wear depth on the surface of the QT-500 metal gradually deepens, and the pit size increases, indicating that the wear area distribution changes from sparse to dense. Specifically, under a 100 N load, the pit depth is about 0.9 μm, and the hole diameter is about 42 μm; under a 120 N load, the pit depth is about 0.7 μm, and the hole diameter is about 36 μm; under a 140 N load, the pit depth is about 1.7 μm, and the hole diameter is about 83 μm. In contrast, the surface of the Fe55 coating metal did not exhibit large-sized pits under the test conditions, showing superior wear resistance.

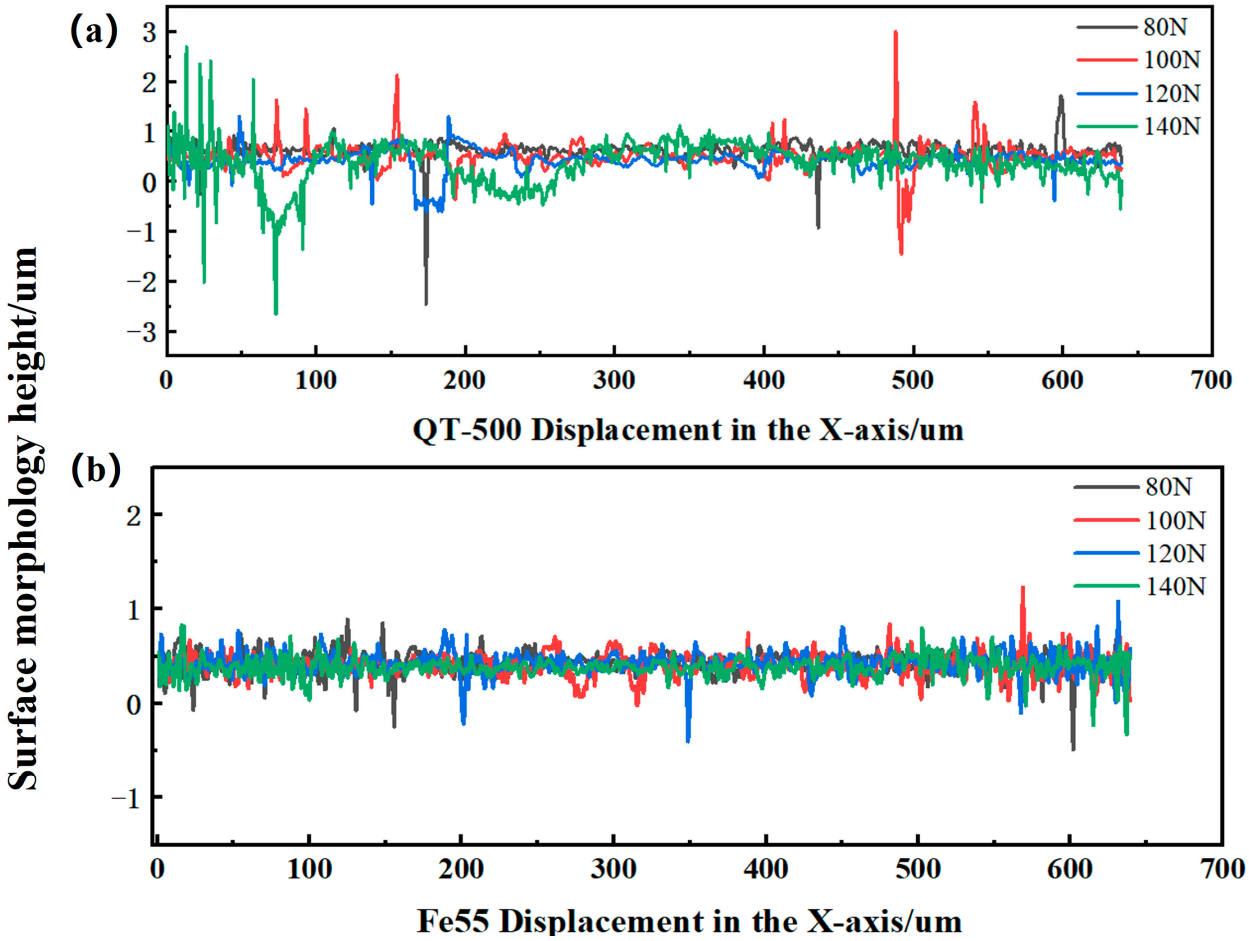


Figure 12. The wear characteristic dimensions of the QT-500 and Fe55 coating. (**a**) The morphological height profile of the QT-500. (**b**) The morphological height profile of Fe55 coating.

As shown in Figure 13, the worn surfaces of QT-500 and Fe55 coating exhibit typical metallic abrasive wear characteristics. Regular furrows are distributed on the surfaces, and

these furrows are parallel to the sliding direction. As shown in Figure 13a,a1, the surface of QT-500 undergoes fatigue damage and brittle spalling due to the repeated action of abrasives, leading to the destruction of the material surface. As shown in Figure 13b,b1, the surface of the Fe55 coating is in good condition and demonstrates excellent wear resistance under abrasive wear conditions.

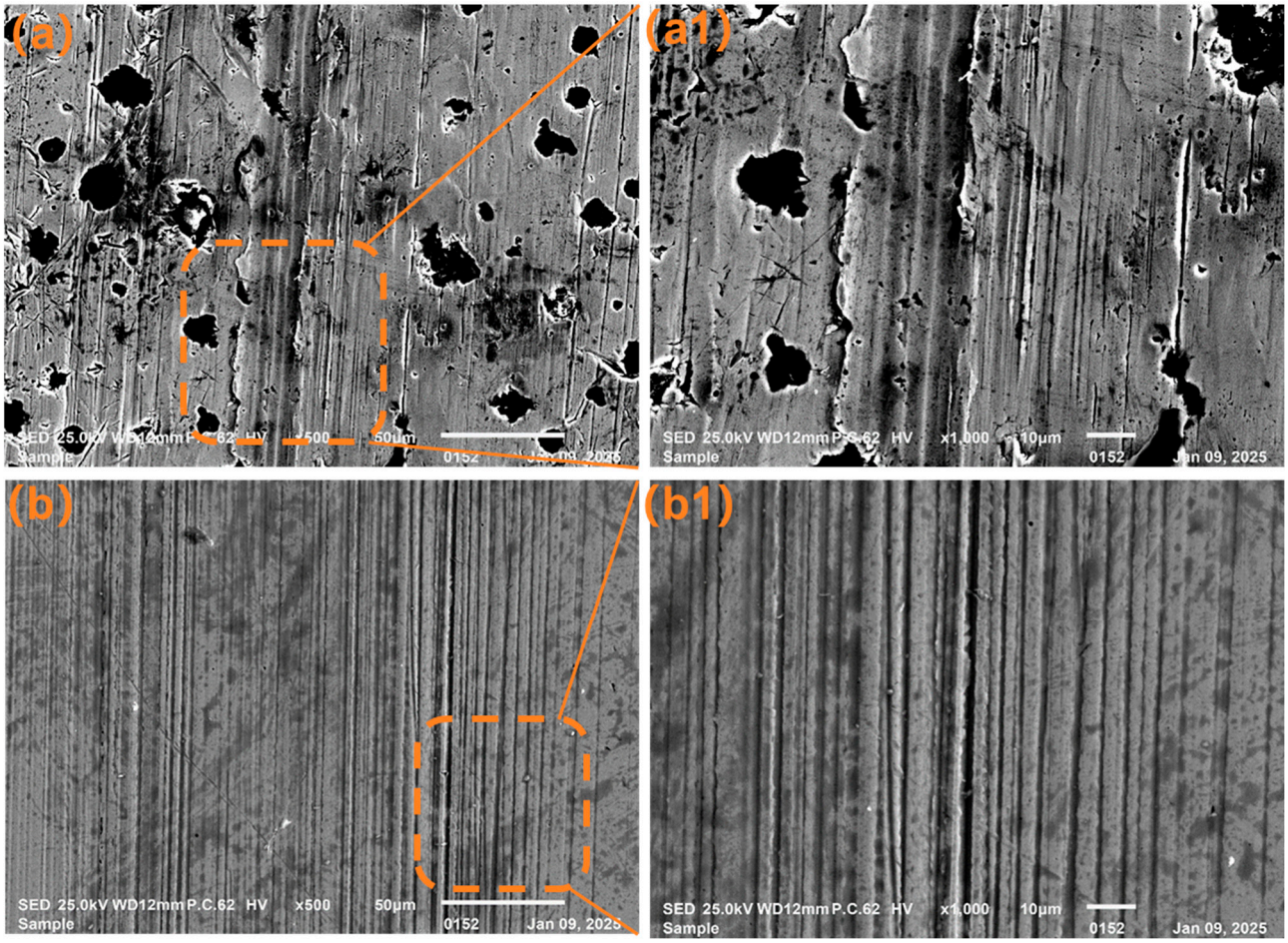


Figure 13. (**a**) Surface wear phenomenon of QT-500 under 140 N. (**b**) Surface wear phenomenon of Fe55 under 140 N.

4. Discussion

4.1. Frictional Properties of Oil-Lubricated Lip Seal Friction Pair Materials

The mechanism of accessory wear in lip seal friction under oil lubrication is illustrated in Figure 14. In Figure 14a, a schematic diagram of the lip seal structure is presented. The primary wear interface occurs between the main lip of the rotating lip seal and the metal shaft. As shown in Figure 14b, during static contact, rubber is exuded onto the metal surface. Generally, this extruded rubber surface can be easily stretched during the relative movement with the metal, leading to deformation and wear of the rubber material, as depicted in Figure 14c.

However, under certain loads, the micro-convex structures on the metal can compress the rubber material, forming a wedge gap. At a specific speed, the presence of lubrication creates a fluid dynamic pressure effect within the wedge gaps, as shown in Figure 14d. This generates a certain pressure between the metal and HNBR, which reduces the wear between the metal and rubber surfaces.

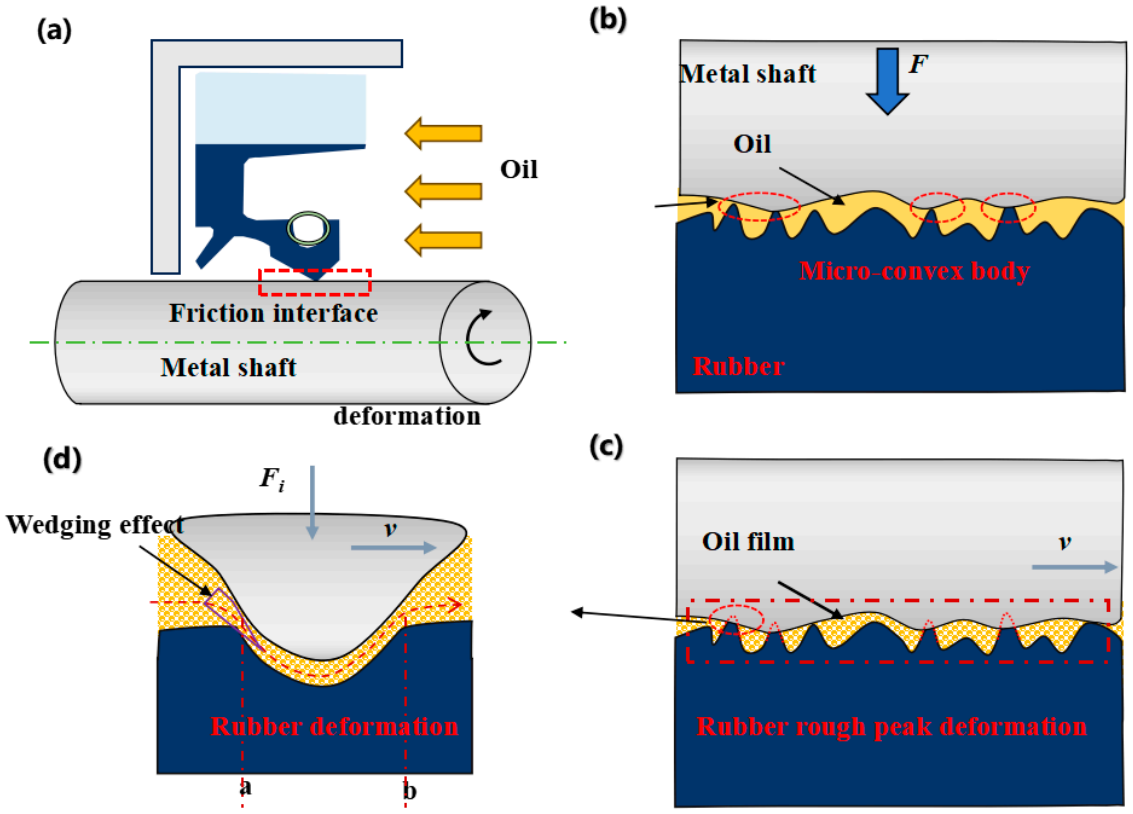


Figure 14. The diagram of soft lubrication mechanism in rubber seals. (**a**) Lip seal and soft contact. (**b**) Surface contact state. (**c**) Oil lubrication friction. (**d**) Hydrodynamic pressure effect.

4.2. Mechanism of Abrasive Wear

In the process of three-body abrasive wear, the motion states of abrasive particles within the tribological interface typically include two main forms: sliding and rolling. These two motion states significantly influence the wear behavior and mechanisms [18,19]. When abrasive particles are involved in the tribological process, they are subject to various forces. The force analysis for sliding and rolling abrasive particles is illustrated in Figure 15d. The forces acting on the HNBR include stress σ or torque M, fluid force τ, frictional resistance F_f provided by the metal specimen, and the hysteresis recovery force of HNBR. When the abrasive particle is rolling, its height in the direction of the plumb line is R, the distance to the metal surface is r_1, and the distance from the center of gravity of the abrasive particle to the HNBR surface is r_2. The metal's hardness is considerably higher than that of the abrasive particle, so the depth of penetration of the abrasive particle into the metal is negligible.

Theoretical research indicates that when a cylinder or sphere rolls on a flat surface, the rolling frictional coefficient is positively correlated with the axial load [20]. The frictional coefficient between a hard particle and a metal surface is almost a constant value, implying that as the axial load increases, the driving force required to roll the particle also increases linearly. In other words, the torque needed to prevent the hard particle from rolling increases faster than the driving torque. There must be a critical value at which the mode of motion of the hard particle transitions from rolling to sliding. As the axial load increases, the proportion of rolling particles gradually decreases, while the proportion of sliding particles gradually increases.

When the axial load is less than 80 N, the friction mechanism is as shown in Figure 15a. Under small loads and specific sliding speeds, due to the hydrodynamic lubrication effect, a lubricating film can be formed between the friction pairs, which to some extent reduces the adhesion wear between the friction pairs. The addition of hard particles also reduces the

local adhesion between rubber and metal to a certain extent. Due to the larger contact gap, there are more hard particles on the contact surface, and the movement mode of the hard particles is mainly rolling, causing small deformations on the HNBR surface. In addition to the grooves on the metal surface, pits formed by the rolling of abrasive particles are also found.

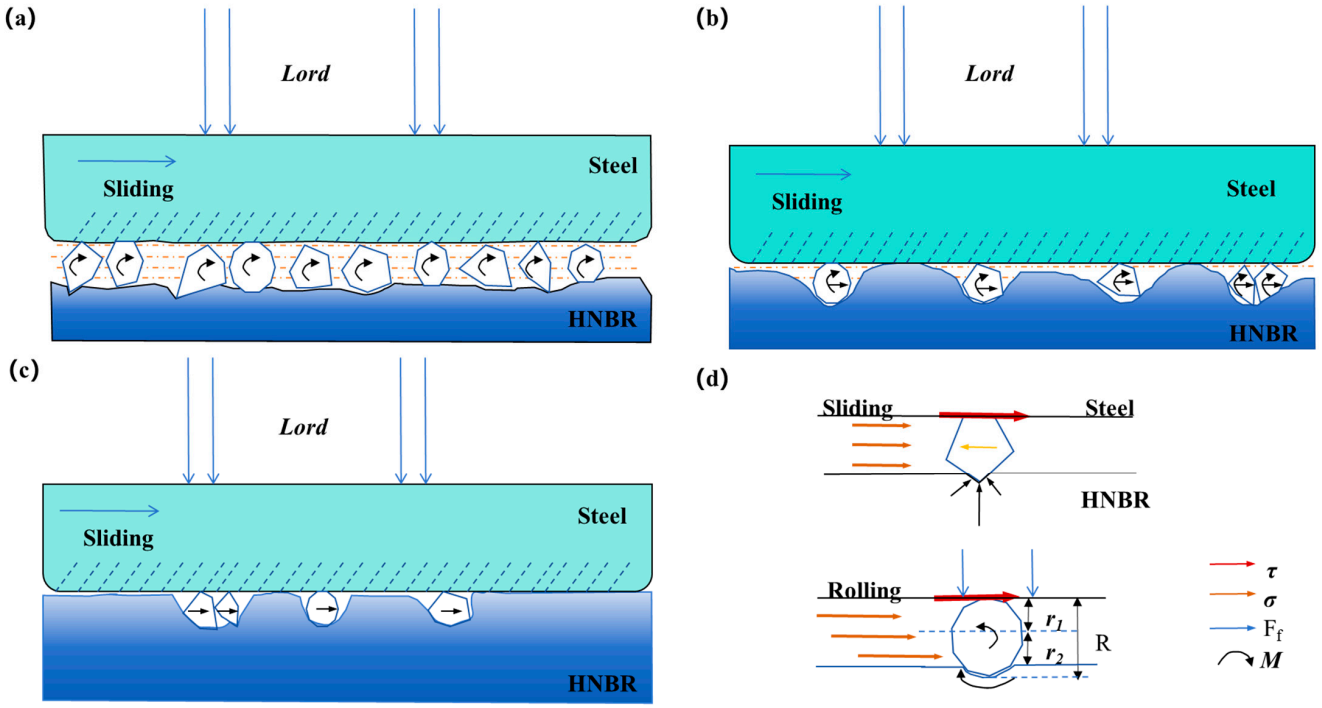


Figure 15. (**a**) Schematic diagram of the friction mechanism under the axial load 80 N. (**b**) Schematic diagram of soft contact under the axial load of 100 N, 120 N. (**c**) Schematic diagram of soft contact under the axial load of 140 N. (**d**) The force analysis of particles at lubricating surface.

When the axial load increases to 100 N or 120 N, the friction mechanism is as shown in Figure 15b. As the axial load increases, the contact gap decreases, the thickness of the lubricating film becomes thinner, the hydrodynamic lubrication effect weakens, and the contact effect between hard particles and the HNBR surface is enhanced. The number of hard particles embedded in the wear surface increases, the lubricating film becomes discontinuous, and the local adhesion effect is enhanced, leading to an increase in adhesion losses. The movement mode of hard particles begins to change from rolling to sliding, causing greater deformation on the HNBR surface. The micro-cutting effect of hard particles on the HNBR surface begins to enhance, continuously plowing grooves on the HNBR surface.

When the axial load increases to 140 N, the friction mechanism was shown in Figure 15c. As the contact gap is further compacted, the angular contact effect between the HNBR surface and hard particles is enhanced, and some areas where the HNBR surface wraps around hard particles are more prone to stress concentration. In some areas, the stress exceeds the strength limit, causing the abrasive particles to puncture the rubber surface and form pits. The abrasive particles will slide and plow along with the rubber in the sliding direction, forming grooves on the metal surface.

5. Conclusions

The tribological properties of rubber seals were studied for offshore wind power facilities. The conclusions are summarized as follows:

- With the increase in axial load, the average frictional coefficient decreases, while the wear loss of HNBR samples increases. With the increase in rubbing time, the frictional coefficient drops first, then rises and finally stabilizes.
- With the increase in axial load, the metal surface wear formed gradually changes from rolling wear mainly in pits to sliding wear mainly in furrows. Laser cladding improved the hardness and wear resistance of the metal surface, which mainly showed furrow wear under high load conditions.
- These results show that laser cladding is an effective surface treatment technology, which can significantly improve the wear resistance of materials under harsh working conditions.

Author Contributions: Conceptualization, G.T., C.Z., Z.W. and X.H.; methodology, G.T.; investigation, G.T., C.Z., Z.W., G.H., J.L. and X.H.; writing—original draft preparation, G.T. and C.Z.; writing—review and editing, all; supervision, G.T.; project administration, G.T.; funding acquisition, G.T. and X.H. All authors have read and agreed to the published version of the manuscript.

Funding: The authors gratefully acknowledge the National Natural Science Foundation of China (52475180, 52105176), the Guangdong Basic and Applied Basic Research Foundation, China (No. 2022A1515240004), and the Program for Guangdong Introducing Innovative and Entrepreneurial Teams (2019BT02Z393).

Data Availability Statement: Data are contained within the article.

Conflicts of Interest: Author Xing Huang was employed by the Guangzhou Mechanical Engineering Research Institute Co., Ltd. Author Guang Jing Huang was employed by the CATO Co., Ltd. The remaining authors declare that the research was conducted in the absence of any commercial or financial relationships that could be construed as a potential conflict of interest.

References

1. Greene, J.S.; Morrissey, M. Estimated Pollution Reduction from Wind Farms in Oklahoma and Associated Economic and Human Health Benefits. *J. Renew. Energy* **2013**, *2013*, 924920. [CrossRef]
2. Artigao, E.; Martín-Martínez, S.; Honrubia-Escribano, A.; Gómez-Lázaro, E. Wind turbine reliability: A comprehensive review towards effective condition monitoring development. *Appl. Energy* **2018**, *228*, 1569–1583. [CrossRef]
3. Faulstich, S.; Hahn, B.; Jung, H.; Rafik, K. Suitable failure statistics as a key for improving availability. In Proceedings of the European Wind Energy Conference, Marseille, France, 16–19 March 2009.
4. Wang, H.; Lu, X.M.; Tian, W.; Lu, J.R. A supporting and repair solution of bearing v-ring for wind power generator accelerator. *Lubr. Eng.* **2014**, *39*, 127–129.
5. Yang, J.; Liu, Z.; Cheng, Q.; Liu, X.; Deng, T. The effect of wear on the frictional vibration suppression of water-lubricated rubber slat with/without surface texture. *Wear* **2019**, *426*, 1304–1317. [CrossRef]
6. Tan, G.B.; Li, J.F.; Li, S.L.; Zhou, C.; Huang, X.; Luo, B.X.; Fan, Y.C.; Liu, D.H. Numerical simulation of high performance lip seal for ultra large offshore wind power equipment. *Mech. Electr. Eng. Technol.* **2024**, *41*, 185–189.
7. Feng, Y.L.; Xiao, P.; Kai, F. Study on microstructure and compressive properties of Fe-C-W-Cr-V-Nb coating with boron addition. *J. Alloys Compd.* **2022**, *904*, 163986. [CrossRef]
8. Qin, C.; He, S.; Zhou, X.; Li, Q.; Li, Q.; Yang, Z. Research on the effect of Nano/Micron SiO_2 particles on actual wear of the main gear box of large-scale mechanical equipment. *Tribol. Lett.* **2023**, *72*, 12. [CrossRef]
9. Zuo, R.; Wang, G.; Hu, G.; Zhao, S.; Wei, G. Tribological properties of hydrogenated nitrile rubber in confrontation with hard particles under different axial loads. *Tribol. Int.* **2021**, *153*, 106649. [CrossRef]
10. Zhou, Z.; Zhou, Q.; Qin, K.; Li, S.; Zhang, K.; Yuan, T.; Sun, W. The Particle Breakage Effect on Abrasive Wear Process of Rubber/Steel Seal Pairs under High/Low Pressure. *Polymers* **2023**, *15*, 1857. [CrossRef] [PubMed]
11. Zhu, L.; Xue, P.; Lan, Q.; Meng, G.; Ren, Y.; Yang, Z.; Xu, P.; Liu, Z. Recent research and development status of laser cladding: A review. *Opt. Laser Technol.* **2021**, *138*, 106915. [CrossRef]
12. Liu, Y.; Ding, Y.; Yang, L.; Sun, R.; Zhang, T.; Yang, X. Research and progress of laser cladding on engineering alloys: A review. *J. Manuf. Process.* **2021**, *66*, 341–363. [CrossRef]
13. Tan, G.; Li, J.; Zhou, C.; Luo, Z.; Huang, X.; Guo, F. Numerical simulation study of high-speed lip seal considering eccentricity. *Ind. Lubr. Tribol.* **2024**, *1*, 25. [CrossRef]

14. Lv, X.R.; Chen, J.C.; Qiao, H.T.; Wang, S.J. Effect of shape of sand grains on wear of nitrile rubber in crude oil with sand and their mechanical behavior. *J. Mater. Res.* **2018**, *321*, 65–72.
15. Qin, K.; Zhou, Q.; Zhang, K.; Li, S.; Lv, M.; Xia, B.; Bai, S. Differences in Wear Tongue Development: Thermal Degrade Effect on the Tribological Behavior of FKM O-Ring Seals. *Tribol. Lett.* **2021**, *69*, 125. [CrossRef]
16. Shen, M.X.; Li, B.; Rong, K.J.; Yuan, C.; Zhang, Z.; Zhang, J. Effect of abrasive size on tribological behavior of rubber sealing pair under water-lubricated conditions. *Tribology* **2020**, *40*, 252–259.
17. Nguyen, Q.B.; Nguyen, D.N.; Murray, R.; Ca, N.X.; Lim CY, H.; Gupta, M.; Nguyen, X.C. The role of abrasive particle size on erosion characteristic soft stainless steel. *Eng. Fail. Anal.* **2019**, *97*, 844–853. [CrossRef]
18. Cozza, R.C. Effect of sliding distance on abrasive wear modes transition. *J. Mater. Res. Technol.* **2015**, *4*, 144–150. [CrossRef]
19. Du, D.S.; Fang, L.; Li, C.X. Investigation of the movement patterns of abrasive in three-body plastic abrasion. *Lubr. Eng.* **2004**, *29*, 66–68.
20. Gang, H.; He, X.; Wang, G.R.; Hu, G.; Zhang, W. Effect of Abrasive Size on Tribological Properties of HNBR for Reciprocating Seal. *Tribology* **2024**, *44*, 1009–1020.

Disclaimer/Publisher's Note: The statements, opinions and data contained in all publications are solely those of the individual author(s) and contributor(s) and not of MDPI and/or the editor(s). MDPI and/or the editor(s) disclaim responsibility for any injury to people or property resulting from any ideas, methods, instructions or products referred to in the content.